# EFFECT OF FIBER CONTENT VARIATION IN PLASTIC HINGE REGION OF REINFORCED UHPC FLEXURAL MEMBERS

**Mandeep Pokhrel [(1)] [*], Yi Shao [(2)], Sarah Billington [(2)] and Matthew J. Bandelt [(1)]**

[(1)] Department of Civil and Environmental Engineering, New Jersey Institute of Technology, USA

[(2)] Department of Civil and Environmental Engineering, Stanford University, USA

[*] Corresponding author: mp595@njit.edu

## ABSTRACT

Ultra-high performance concrete (UHPC) is used for the construction of resilient structures that can sustain dynamic loadings such as blast, impact, and earthquake loadings, among others. In structural components subjected to such loading, it is essential to ensure the formation of a ductile plastic hinge mechanism for suitable load transfer mechanisms and global stability of the structure. Experimental research is needed to understand the formation of plastic hinges in UHPC materials and the impact of plastic hinges on the rotation capacity of reinforced UHPC structural components. The study presented herein aims to understand the spread of plasticity and formation of plastic hinge regions in reinforced UHPC flexural members. Two reinforced UHPC beams with variation in fiber volume fraction (i.e., $V_f$ = 1% and 2%) were subjected to monotonic loading. The test results demonstrated that the reinforcement plasticity length increased by 26% with a decrease in fiber volume fraction from 2% to 1%. The plastic hinge region of specimens with 2% fiber content had crack localization within the maximum moment region, whereas the specimen with 1% fiber content had a more uniformly distributed localized crack pattern. Further, analytical models and a recently proposed equivalent plastic hinge length equation were used to predict and compare the flexural strength and rotation values at various damage states.

**KEYWORDS:** plastic hinge length, fiber content, reinforced UHPC, ultimate rotation capacity

## 1. INTRODUCTION & BACKGROUND

Ultra-high performance concrete (UHPC) is an advanced cement-based composite material designed with optimal particle packing density, such that, it possesses extremely high compressive strength (> 120 MPa without heat treatment) and enhanced durability properties [1]. When combined with short discontinuous fibers, UHPC materials have high tensile strength (> 5 MPa), tensile fracture toughness, and ductile strain-hardening behavior under uniaxial tension tests [1]. The mechanical properties of UHPC have led researchers and engineers to perform a large number of proof-of-concept investigations under extreme loading conditions such as blast, impact, earthquake, and fire [2]. In high seismic zones, researchers are especially interested in the applicability of UHPC in plastic hinge regions of structural components undergoing large inelastic deformations [3]. Various classes of high performance fiber reinforced cementitious composites (HPFRCCs) have already been effectively used in plastic hinge region of structural components such as coupling beams, columns, and bridge piers in recent years [4].

The use of UHPC in the plastic hinge regions of structural components can enhance the load carrying capacity, ductility, and energy absorption capacity because the mechanical properties of UHPC can prevent premature failure associated with damage in plastic hinge regions, as is typically observed in structural components made with conventional concrete (e.g., spalling of cover, buckling of rebar, shear cracks, etc.).

Structural components can be engineered to improve the damage tolerance of structures by using UHPC in plastic hinge region, while using conventional concrete in the remaining portions of the component [3]. Such an approach can minimize the high cost associated with UHPC while reducing the overall life cycle cost (i.e., maintenance and repair cost) of the structure. To optimize the initial construction cost, the fiber volume fraction used in a UHPC material can be reduced; however, the influence of such a reduction on structural ductility and performance of plastic hinge regions is not well understood. A previous numerical study conducted using a wide range of HPFRCC materials indicated that the tensile strength and ductility of the matrix can significantly alter the amount of damage and the length of the plastic hinge region in reinforced HPFRCC flexural members [5,6]. Therefore, the use of low fiber content in regions undergoing large displacement reversals may result in an undesired failure mechanism (e.g., shear cracking) without the formation of a ductile plastic hinge mechanism.

Other experimental and numerical studies have shown that the flexural behaviour of reinforced HPFRCCs (including UHPC) in terms of crack progression, reinforcement plasticity, and failure mechanism is significantly different than conventional reinforced concrete structural components [7-10]. Specifically, the failure mode of flexural members is found to be predominantly through the fracture of longitudinal reinforcement rather than compression crushing of an HPFRCC matrix. This is due to a *crack localization* phenomenon observed in reinforced HPFRCC structural components, wherein the plastic damage concentrates in the vicinity of a single or few flexural cracks. Several bond experiments with lap splice beam specimens have shown that higher bond strength of HPFRCC matrix restraints the formation of splitting cracks which leads to such a phenomenon [11-13]. Further, tension stiffening experiments of reinforced HPFRCC prisms have shown that there is localized strain hardening in longitudinal reinforcement at such localized cracks [14,15]. Localized hardening of steel reinforcement can provide a strengthening mechanism at the critical section of reinforced HPFRCC flexural members, until the member loses its load-carrying capacity by reinforcement fracture.

Shao and Billington [16] recently conducted an experimental study with reinforced UHPC beams consisting of two different reinforcement ratios ($\rho$ = 0.96% and 2.10%). The study showed that there can be two different failure paths in reinforced UHPC beams depending on the amount of longitudinal reinforcement used. The use of low reinforcement ratio led to *failure after crack localization* failure path in which there were three major damage states: yielding, crack localization, and rebar fracture. The use of a high reinforcement ratio led to *failure after gradual strain hardening* failure path in which the intermediate damage state changed from crack localization to compression crushing (or softening). Compared to specimens that fail after crack localization, specimens that fail after gradual strain hardening show higher ductility and more failure warnings. The flexural failure paths and various damage states are found to be pre-dominantly dependent on longitudinal reinforcement and matrix property based on similar experimental studies carried out on other HPFRCC materials [10,17].

Although many experimental studies have investigated the flexural behavior of reinforced UHPC beams, their specimens mostly fail after crack localization [16, 17]. There is limited experimental study in the literature dedicated to investigate the reinforcement plasticity distribution, curvature distribution, UHPC surface strain variation, and damage propagation in plastic hinge region of UHPC beams that fail after gradual strain hardening. Further, the influence of fiber content variation on various parameters, as mentioned above, is important to understand the component flexural behaviour, especially the maximum load carrying capacity, deformation capacity, and structural stability of components constructed with such material and cross-section property. Moreover, a mechanics-based analytical approach is adopted in the study, to predict strength and rotation capacity of the such

specimens, which provides a simplified way for the practicing engineers to model and design such components in large structural systems.

To that end, an experimental study consisting of two reinforced UHPC beams with 1% and 2% fiber volume fraction ($V_f$) were tested under a four-point bending test setup. Based on recent experimental studies [16,17], these two beams were designed to fail after gradual strain hardening by adopting a high reinforcing ratio of 2.10%. The flexural response, length of reinforcement yielding, inelastic curvature distribution, crack distribution, and strain variation within the maximum moment region were investigated. Analytical models and a recently proposed equivalent plastic hinge length equation for ductile concrete composites were used to predict flexural strengths and rotation values at various damage states.

## 2. EXPERIMENTAL PROGRAM

### 3.1. Materials, mixture proportions, and mechanical tests

Two types of mixture proportions were used in the experiment as listed in Table 1. The propriety pre-mix blend contained a mixture of cement, quartz, and silica fume. There were three types of admixtures used to improve the workability of UHPC during the casting period. Standard smooth steel fibers with a diameter of 0.2mm and length of 13 mm were used in both mixtures. The naming convention of the beam specimens were based on the percentage of fiber volume fraction used in each specimen. Therefore, UHPC-1% denotes the specimen with a fiber volume fraction of 1% and UHPC-2% indicates the specimen containing a fiber volume fraction of 2%. The materials were mixed in a horizontal shear mixer and poured from one end of the beam mold until the mold was filled up to the full height.

**Table 1.** Mixture proportions (per $\boldsymbol{m^3}$)

| Specimen | Premix Blend [kg] | Water [kg] | Fibers [% Vol.] | Admix. A [kg] | Admix. B [kg] | Admix. C [kg] |
|---|---|---|---|---|---|---|
| UHPC-1% | 1939 | 194 | 1.0 | 20 | 26 | 28 |
| UHPC-2% | 1960 | 196 | 2.0 | 20 | 26 | 28 |

All UHPC specimens were moist cured and tested at 56±3 days of casting. The representative results of mechanical tests have been tabulated in Table 2. Both compression and flexural tests of the two types of UHPC mixtures were conducted in accordance with ASTM C1856-17 [18]. Cylindrical specimens of diameter 75 mm and height 150 mm were prepared and tested to obtain compressive strength and modulus of elasticity. Four-point bending tests were performed on UHPC prisms with a cross section dimension of 75 x 75 mm and a length of 300 mm to obtain the equivalent bending stress versus displacement response as shown in Figure 1 (a).

**Table 2.** Mechanical properties

| Description | $f_t$[1] [MPa] | $G_f$[1] [MPa-mm] | $f_c'$ [MPa] | $E$ [GPa] | $f_y$ [MPa] | $f_u$ [MPa] | $\varepsilon_u$ [%] | $\varepsilon_f$ [%] |
|---|---|---|---|---|---|---|---|---|
| UHPC-1% | 5.2 | 6.4 | 170 | 41.6 | - | - | - | - |
| UHPC-2% | 9.2 | 6.7 | 180 | 42.5 | - | - | - | - |
| Longitudinal Rebar (#6) | - | - | - | 190 | 470 | 780 | 10 | 18[2] |
| Transverse Rebar (#3) | - | - | - | 200[3] | 510[3] | - | - | - |

[1]Obtained using inverse analysis; [2]Extrapolated value; [3]Manufacturer listed value

A series of inverse analyses were conducted using two-dimensional finite element simulations to estimate the tensile properties of the two UHPC mixtures. The inverse analysis scheme adapted in this study has been successfully implemented by other researchers in the past to characterize the tensile stress-strain curve without resorting to the direct tension test [9,10,17]. A total strain-based fixed-crack constitutive model was used with trial multilinear tensile stress-strain curve as an input to the numerical model. It can be observed from Figure 1 (a) that the simulated flexural response from inverse analysis closely approximates the experimental flexural behaviour of unreinforced UHPC prisms. The corresponding tensile strength ($f_t$) and tensile fracture energy ($G_f$) of the mixtures are listed in Table 2, which can be used in lieu of tensile parameters obtained from direct tension test to investigate the flexural behavior and plastic hinge region of reinforced UHPC beams tested in this study. ASTM A615 Grade 60 steel with a diameter of 19 mm was used as longitudinal reinforcing bar in both UHPC-1% and UHPC-2% specimens. A uniaxial tension test was conducted using an extensometer of gauge length 50 mm to obtain characteristic tensile properties of the longitudinal reinforcement as listed in Table 2. Transverse reinforcement of Grade 60 steel with manufacturer listed yield strength of 510 MPa was used in both specimens.

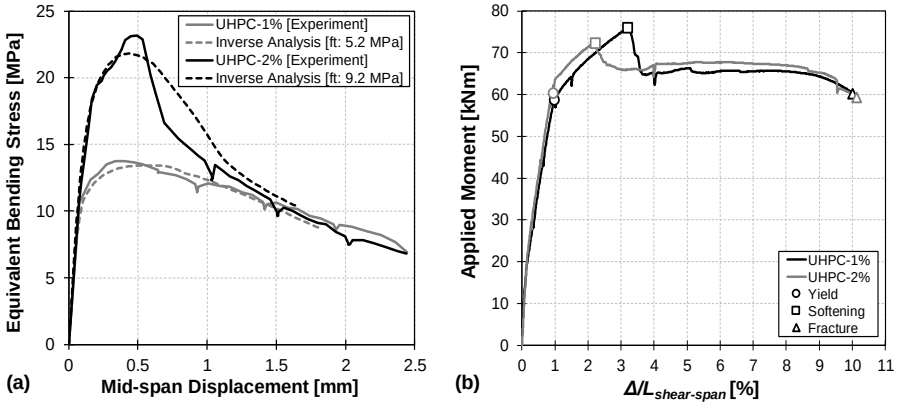


**Figure 1.** (a) Equivalent bending stress vs. mid-span displacement of unreinforced UHPC beams (b) Applied moment vs. drift response of two reinforced UHPC beams with different damage states

### 3.2. Test specimens, setup and instrumentation

Two reinforced UHPC beam specimens were tested using a four-point bending setup as shown in Figure 2(a). A digital image correlation (DIC) system was used to assess variations in strain in the constant moment region of 200 mm between the two point loads. Since the DIC system could not be extended further due to laboratory constraints, a series of linear variable displacement transducers (LVDTs) were used to measure the vertical displacement along one side of the beam to a distance of 200 mm from the center line of the right point load towards the roller support.

Figure 2 (b-c) shows the design of the beam with longitudinal reinforcement layout, transverse reinforcement layout, location of strain gauges, and cross-section details. The strain in the bottom longitudinal reinforcement was measured at five locations by attaching post-yield strain gauges (YEFLA-2-3LJC-F from Tokyo Measuring Instruments Lab) with a maximum measurement capacity of 10%. Two longitudinal reinforcing bars of diameter 19 mm were used in the top and bottom sides of the cross section resulting into a tensile longitudinal reinforcement ratio of 2.10%. Transverse reinforcement was provided at a spacing of one-half of the effective depth (i.e., $d/2$) with bars of diameter 9.5 mm. The specimens were subjected to a monotonic loading at the rate of 0.097 mm/s until they lost their load carrying capacity by fracture of the tensile longitudinal reinforcement.

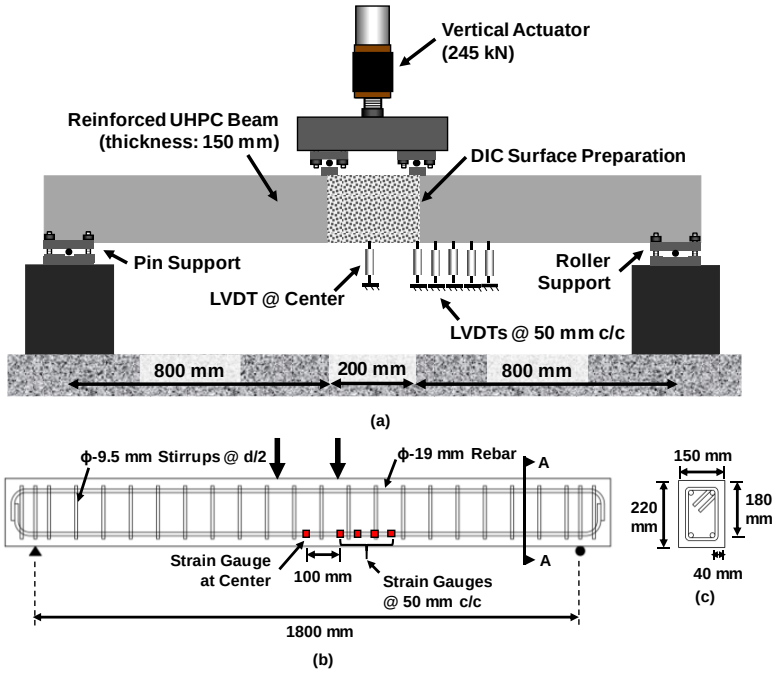


**Figure 2.** (a) Test setup of reinforced UHPC beams with location of DIC surface and LVDTs (b) Specimen design detail with location of strain gauges (c) cross section at A-A

## 3. RESULT & DISCUSSION

### 3.1. Moment-drift response

The applied moment versus drift response of the two specimens with various damage states is shown in Figure 1 (b). Drift is expressed in percentage (%) and is calculated by normalizing the vertical displacement at mid-span by the shear-span length ($\Delta/L_{shear-span}$). The initial elastic response of both beams including stiffness, moment at yield and drift at yield are similar. The beams were assumed to yield when the strain in the tensile reinforcement at mid-span reached the yield strain ($\varepsilon_y$) of 0.2772%. At yield, the moment and drift capacities are similar because of the use of the same reinforcement ratio ($\rho$ = 2.10%) in both beams. The strength and drift capacities at yield are less sensitive to variations in tensile strength of the matrix (or fiber volume fraction) in specimens with higher reinforcement ratios compared to specimens with lower reinforcement ratios [5]. After yield, the flexural load carrying capacity increased in both specimens due to the combination of fiber bridging action and localized hardening of the tensile reinforcement. The post-yield stiffness of both beams were similar; however, the nominal moment ($M_n$) capacity (i.e., peak moment capacity) of UHPC-2% (72.2 kNm) was found to be lower than UHPC-1% (75.9 kNm). It was anticipated that the UHPC-2% specimen, which has twice the fiber content and a higher tensile strength than UHPC-1% beam, would have a higher nominal moment capacity than UHPC-1% specimen. However, a higher rate of post-yield strain accumulation in the compression zone of UHPC-2% specimen was observed (Figure 5 (a)). This led to earlier softening of the compression matrix and a lower flexural load carrying capacity in UHPC-2% specimen than in UHPC-1% specimen. The drift of UHPC-2% specimen at the nominal level is lower than the

drift of UHPC-1% by 31% because of the rapid strain concentration in the compression zone of the UHPC-2% specimen. For example, at 2.2% drift level, the compression zone strain ($\varepsilon_c$) in UHPC-2% beam was found to be 35% higher than in UHPC-1% beams (i.e., $(\varepsilon_c)_{UHPC\text{-}2\%}$ = 0.42% whereas $(\varepsilon_c)_{UHPC\text{-}1\%}$ = 0.31% as shown in Figure 5 (a)) as further discussed in Section 3.5. Both specimens were able to achieve large deformations without significantly losing load carrying capacity because the hardened bottom longitudinal reinforcement acted as the tensile component of the flexural couple before reaching the fracture point. This failure mechanism with gradual strain hardening of tensile reinforcement is mostly found in reinforced HPFRCC flexural members with high reinforcement ratios [17]. It is interesting to note that the variation of fiber content did not influence the value of ultimate drift capacity ($(\Delta/L_{shear-span})_{UHPC\text{-}1\%}$ = 10.02% and $(\Delta/L_{shear-span})_{UHPC\text{-}2\%}$ = 10.15%). The results indicates that the ultimate rotation or drift capacity of reinforced UHPC beams with high longitudinal reinforcement (i.e., $\rho > 2\%$) is not sensitive to variation in fiber volume fraction compared to the beams with low to moderate reinforcement ratio (i.e., $1\% < \rho < 2\%$).

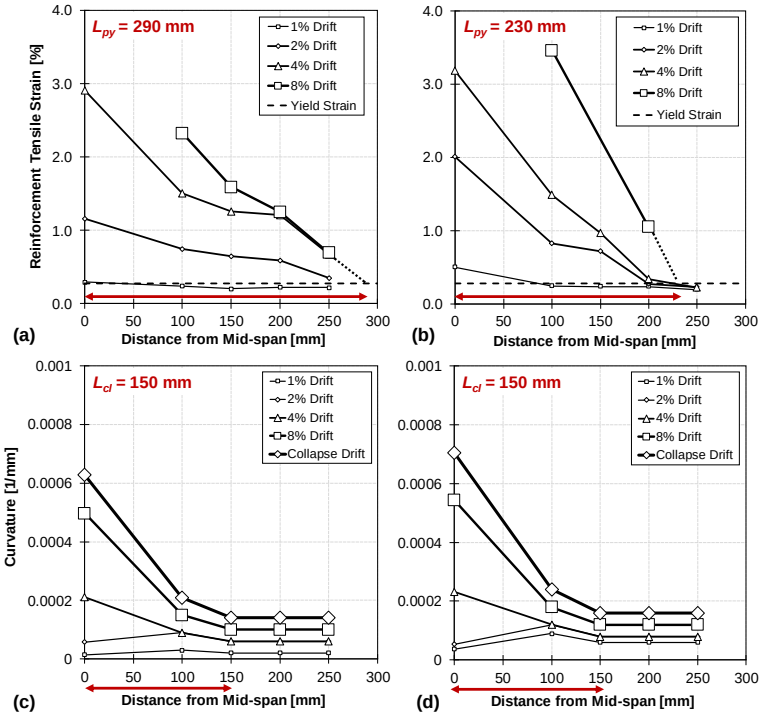


**Figure 3.** Longitudinal reinforcement tensile strain vs. distance from mid-span at various drift levels for (a) UHPC-1% specimen and (b) UHPC-2% specimen Curvature vs. distance from mid-span at various drift levels for (c) UHPC-1% and (d) UHPC-2% specimens

### 3.2. Strain distribution

Figure 3 (a-b) presents the variation of reinforcement tensile strain from mid-span to the right side of the specimens (up to 250 mm). At 1% drift, it can be observed that the UHPC-1% specimen had a reinforcement yielding length, $L_{py}$, of 50 mm, whereas the longitudinal reinforcement yielded over a length of 90 mm in UHPC-2% specimen. However, $L_{py}$ in the UHPC-1% specimen increased at higher drift level compared to UHPC-2% specimen because of the opening of flexural cracks along a longer

span length as shown in Figure 4. The fiber bridging action and matrix tensile strength of UHPC-1% specimen is lower than the UHPC-2% specimen. The lower strength of UHPC-1% allowed cracks top easily open at high drift levels and plasticity distributed uniformly over a longer length of reinforcement. The length of reinforcement yielding remained constant at higher drifts in both specimens as the inelastic strain concentration mostly occurred near a dominant crack location as was observed in previous studies involving reinforced HPFRCC flexural members [9,19]. At 8% drift level, the length of reinforcement yielding region in UHPC-1% specimen ($L_{py} = 290\ mm$) was longer than UHPC-2% specimen ($L_{py} = 230\ mm$). These results suggest that the plastic hinge length in beams with higher fiber content (or higher tensile strength and matrix toughness) are shorter than those with lower fiber content (or lower tensile strength and matrix toughness). This is also in agreement with the length and type of cracking pattern shown in Figure 4 and further discussed in Section 3.4.

### 3.3. Curvature distribution

Curvature distribution along the span of the specimens were calculated using the vertical displacements data obtained from the six LVDTs. Mathematically, curvature at a section can be approximated using the elastic deflection theory as shown in Eq. (1).

$$\phi = \frac{d\theta}{ds} \cong \frac{d\theta}{dx} = \frac{\theta_{i+1} - \theta_i}{distance\ between\ LVDTs} \tag{1}$$

Where $\theta_i$ and $\theta_{i+1}$ are the angles at sections $i$ and $i+1$. These angles can be computed using the vertical displacements obtained from LVDTs along the span of the beam. Due to the opening of localized cracks at higher drifts, the recorded vertical displacement data at some locations were estimated using a trendline. Figure 3 (c-d) shows curvature distribution from mid-span to the right side of the specimens at incremental drift levels. At a lower drift level (1% or 2%), the curvature is maximum below the point load, which is the assumed hinge location under four-point bending setup. However, at larger drift levels (4% or more) the curvature is larger at mid-span because of the opening of a major crack at mid-span, such that the section at mid-span deforms more than the section below the point load as seen from the crack pattern at in Figure 4. The overall trend of the curvature is similar to the theoretical curvature under four-point bending test where the curvature is maximum near the mid-span and sharply decreasing away towards the support. The curvature localization region ($L_{cl}$) was 150 mm in both the specimens indicating there was no substantial effect of fiber content variation in curvature distribution of reinforced UHPC flexural members with high reinforcement ratios.

### 3.4. Crack pattern in plastic hinge region

Figure 4 shows the crack pattern and location of reinforcement fracture in UHPC specimens at impending collapse level drift (i.e., $(\Delta/L_{shear-span})_{UHPC\text{-}1\%}$ = 10.02% and $(\Delta/L_{shear-span})_{UHPC\text{-}2\%}$ = 10.15%). Both specimens contained multiple fine distributed cracks without any flexural crack localization up to 1% drift level. However, after yielding of tensile reinforcement, flexural cracks slowly began to open as the fiber-bridging action declined in some of the cracks. Four major flexural cracks widened in both specimens, but the major cracks were evenly spaced in UHPC-1% specimen compared to UHPC-2% specimen as shown in Figure 4. Major cracks widened in the region away from maximum moment in the UHPC-1% specimen because the cracks could open at lower flexural load due to a lower tensile strength and fracture energy of UHPC-1% matrix. In UHPC-2% specimen, major cracks were confined to the maximum moment region and damage was pre-dominantly localized in a single crack (i.e., crack number 3). As crack number 3 widened, rebar plastic strain in the vicinity of that crack concentrated at a higher rate in the UHPC-2% specimen as compared to the UHPC-1% specimen (Figure 5 (b)) as further discussed in Section 3.5. The distance between the extreme minor and major cracks were found to be longer in UHPC-1% specimen ($L_{minor\ cracks}$ = 1350 mm and $L_{major\ cracks}$ = 420 mm) compared to UHPC-2% ($L_{minor\ cracks}$ = 935 mm and $L_{major\ cracks}$ = 240

mm) which can be attributed to the comparatively weaker matrix and fiber-bridging action in UHPC-1% specimen compared to UHPC-2% specimen.

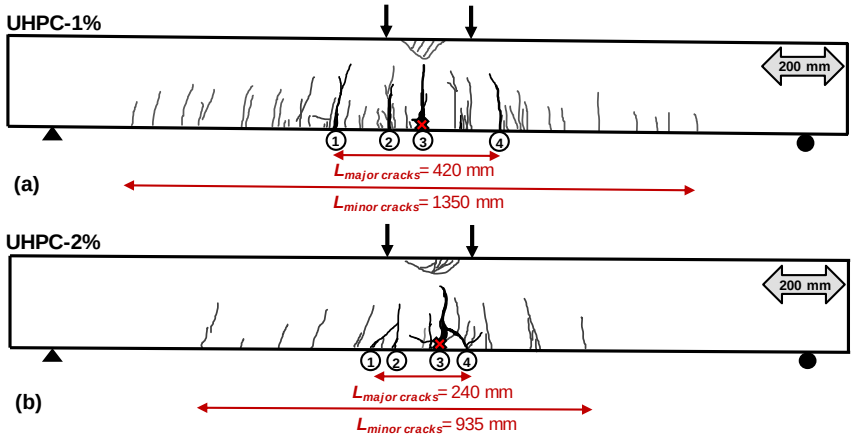


**Figure 4.** Crack pattern in (a) UHPC-1% and (b) UHPC-2% specimens at impending collapse

### 3.5. Variation of strain in maximum moment region

Figure 5 shows the variation of compression and tension strain at mid-span with incremental drift levels. The slope of the lines indicates the rate of strain accumulation in the compression zone (Figure 5 (a)) or in the tensile reinforcement (Figure 5 (b)) at mid-span. After yielding of the specimens, the rate of compression strain accumulation in the UHPC-2% specimen became marginally higher compared to the UHPC-1% specimen because the high tensile strength matrix attracts larger forces at smaller deformation level. Further, higher bond strength in UHPC-2% specimen restricted the formation of splitting cracks, causing early rebar hardening over a small deboned length. The hardening led to widening of a mid-span crack and rapid strain concentration in the tensile longitudinal reinforcement in UHPC-2% specimen at a lower drift level as shown in Figure 5 (b). For example, the strain in the tensile reinforcement at 2% drift level in UHPC-2% specimen was 2.00% and that in UHPC-1% specimen was 1.16%. The effect of this rapid strain variation caused softening of UHPC-2% beam at a lower drift level compared to UHPC-1% beam $((\Delta/L_{shear-span})_{UHPC\text{-}1\%}$ = 3.2% and $(\Delta/L_{shear-span})_{UHPC\text{-}2\%}$ = 2.2%). After softening of the specimens, the compression strain accumulation rate in the UHPC-1% specimen increased compared to the UHPC-2% specimen. The difference in compression strain at the same drift level decreased progressively at higher drift levels. The localized hardening strain in tensile reinforcement at mid-span of the UHPC-2% specimen was much higher compared to the UHPC-1% specimen at the same drift levels. For instance, the strain in tensile reinforcement at 4% drift level in UHPC-2% specimen was 4.72% and that in UHPC-1% specimen was 2.91%. It was anticipated that the UHPC-2% would fail earlier by fracture of reinforcement based on this trend. However, UHPC-2% had a similar deformation capacity as UHPC-1% as discussed in Section 3.1. Further investigation is required to understand the failure mechanism at higher strain levels using post-yield strain gauges of a larger strain capacity.

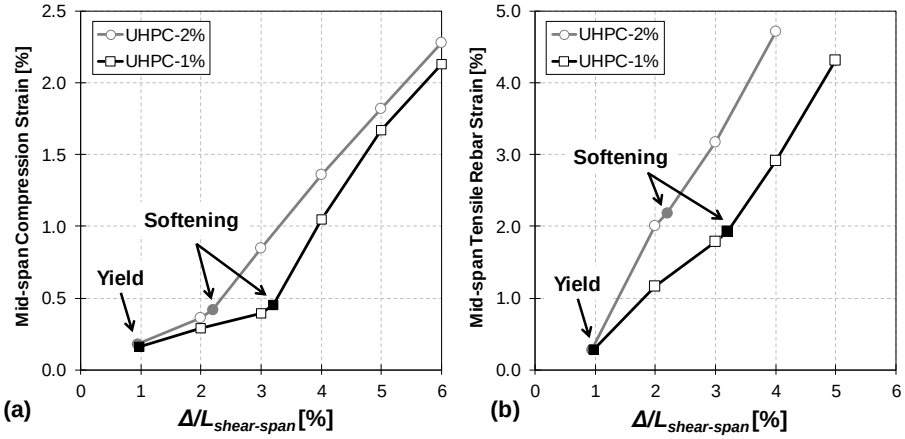


**Figure 5.** (a) Mid-span compression strain vs. drift and (b) mid-span longitudinal tensile reinforcement strain vs. drift

### 3.6. Prediction of flexural strength and rotation capacity

The flexural behavior and failure mechanism of reinforced HPFRCC is significantly different than the conventional reinforced concrete as demonstrated by several experimental studies [7-10]. A recently proposed analytical model (Figure 6) was used to predict flexural strength and rotation capacity at different damage states [10,20]. The predictability of the analytical model was measured by comparison with the experimentally obtained values. The flexural strengths and curvatures at various damage states were computed assuming *linear strain distribution* and using cross section properties of the specimens. The beams were assumed to reach the yield level when the tensile reinforcement strain reached the yield value (i.e., $\varepsilon_y$). The analytical model shown in Figure 6(b) considers a tensile stress block contribution which is ignored in the flexural calculation of conventional concrete components. Elastic deflection theory was used to compute yield rotation using the yield curvature value as shown in Eq. (2). It can be observed from Table 3 that the prediction ratio of both the parameters are close to 1.00, which indicates that the analytical formulation can be successfully used to compute yield rotation and moment capacity of reinforced UHPC flexural members.

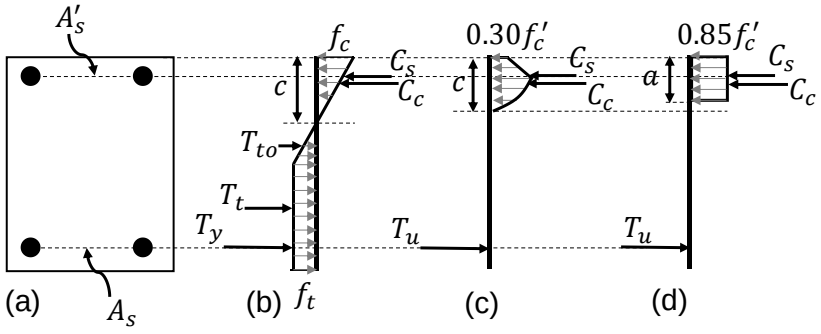


**Figure 6.** Analytical model for section analysis (a) cross-section (b) stress distribution at yield level [20] (c) stress distribution at nominal level using modified Hognestad stress block [10] (d) simplified stress distribution at nominal and ultimate level using Whitney stress block [20].

**Table 3.** Comparison of experimental and analytical results at yield level

| Specimen | Yield Rotation [rad] | | | Yield Moment [kNm] | | |
|---|---|---|---|---|---|---|
| | Exp. | Ana. | Ana./Exp. | Exp. | Ana. | Ana./Exp. |
| UHPC-1% | 0.0098 | 0.0095 | 0.97 | 58 | 53 | 0.92 |
| UHPC-2% | 0.0095 | 0.0098 | 1.03 | 60 | 60 | 1.00 |

Two analytical models were used to estimate the nominal moment capacity: one with modified Hognestad compression stress block (Figure 6(c)) and the second with simplified Whitney compression stress block (Figure 6(d)). Both models considered localized hardening of the reinforcement bar as observed in tension stiffening experiments [14,15]. The beams were assumed to the reach nominal level when the strain in the compression zone reached 3% [10] or tensile reinforcement strain reached ultimate value ($\varepsilon_u$) [20]. It can be observed from Table 4 that the nominal moment predictability using a modified Hognestad stress block is better compared to the use of simplified rectangular Whitney stress block; however, both give reasonable estimates of strength.

**Table 4.** Comparison of experimental and analytical results at nominal and ultimate level.

| Specimen | Nominal Moment [kNm] | | | | | Ultimate Rotation [rad] | | |
|---|---|---|---|---|---|---|---|---|
| | Exp. | Ana.[1] | Ana.[2] | Ana./Exp.[1] | Ana./Exp.[2] | Exp. | Ana. | Ana./Exp. |
| UHPC-1% | 76 | 75 | 80 | 0.98 | 1.06 | 0.1002 | 0.083 | 0.83 |
| UHPC-2% | 72 | 75 | 81 | 1.03 | 1.12 | 0.1015 | 0.060 | 0.59 |

[1]Figure 6(c) [10]; [2]Figure 6(d) [20]

The ultimate rotation capacity was computed using Eq. (2).

$$\theta_u = \theta_y + \theta_p = \frac{1}{2}\phi_y L_s + (\phi_u - \phi_y)L_p \tag{2}$$

Where $L_s$ is the shear span length (mm), $\phi_y$ and $\phi_u$ are the section curvatures of the structural member at yield level ($mm^{-1}$) and collapse level ($mm^{-1}$), respectively. In the above equation, $L_p$ is the equivalent plastic hinge length (mm), which was computed using a recently developed expression based on a range of HPFRCC materials as shown in Eq. (3) [20].

$$L_p = 0.02L_s + \frac{0.24\rho f_y}{f_t} \tag{3}$$

Where $\rho$ is the longitudinal reinforcement (%), $f_y$ is the yield stress (MPa), and $f_t$ is the tensile strength of UHPC mixture (MPa). The analytical framework underestimated the ultimate rotation capacity in both specimens (Table 4). The reason for this discrepancy is the underestimation of equivalent plastic hinge length values for reinforced UHPC specimens tested in this experiment. The expression shown in Eq. (3) was developed using reinforced HPFRCC beams with typical reinforcement ratio (i.e., $0.70\% < \rho < 1.90\%$) and a maximum tensile strength of 8 MPa. As such, the majority of the specimens followed the *failure after crack localization* path with damage localization in a dominant crack. In the current experiment, both the specimens followed *failure after gradual strain hardening* failure path due to the use of a high reinforcement ratio. The damage was uniformly distributed over longer length as seen from the crack patterns. Therefore, there is a need to further improve the plastic hinge length expression for highly reinforced UHPC beams (i.e., $\rho > 2.0\%$) using a more rigorous parametric investigation.

## 4. CONCLUSIONS

This study provides valuable insight about the formation of plastic hinges with variation in fiber volume fraction. The following conclusions can be drawn from this study:

- The variation in fiber content does not impact ultimate rotation capacity in reinforced UHPC beams with high longitudinal reinforcement ratio ($\rho$ > 2.0%).
- The length of plasticity in the longitudinal reinforcement increases with a decrease in fiber volume fraction because of the formation of multiple distributed flexural cracks along the plastic hinge region.
- Distribution of visible cracks in the specimens indicated that the damage is much more localized in specimens with higher fiber content ($L_{major\ cracks}$ = 240mm) than those with low fiber content ($L_{major\ cracks}$ = 420mm) because the UHPC matrix with high fiber content had higher tensile strength, bond strength, and fracture energy which restrained the formation of splitting cracks and prevented opening of additional flexural cracks.
- A parametric study with a wider variation in fiber content at high reinforcement ratios is necessary to further improve a recently developed plastic hinge length expression such that ultimate rotation capacity can be computed with higher accuracy.

## ACKNOWLEDGEMENTS

The authors gratefully acknowledge the financial support from the John A. Reif, Jr., Department of Civil and Environmental Engineering at New Jersey Institute of Technology and John A. Blume Earthquake Engineering Center at Stanford University. The authors would also like to recognize King Packaged Materials Company, Boisbriand, QC for providing materials necessary for the tests.

## REFERENCES

[1] Graybeal, B. A., 'Material property characterization of ultra-high performance concrete', FHWA, Virginia, USA, Tech. Rep. No. FHWA-HRT-06-103. (2006) 1-176.

[2] Yoo, D. and Yoon, Y., 'A review on structural behavior, design, and application of ultra-high-performance fiber-reinforced concrete', *International Journal of Concrete Structures and Materials*. **10** (2) (2016) 125-142.

[3] Ichikawa, S., Matsuzaki, H., Moustafa, A., Elgawady, M. A., and Kawashima, K., 'Seismic-resistant bridge columns with ultra high-performance concrete segments', *Journal of Bridge Engineering*. **21** (9) (2016) 04016049.

[4] Rokugo, K., Kanda, T., Yokota, H. and Sakata, N., 'Applications and recommendations of high performance fiber reinforced cement composites with multiple fine cracking (HPFRCC) in Japan', *Materials and Structures*. **42** (9) (2009) 1197-1208.

[5] Pokhrel, M., and Bandelt, M. J., 'Material properties and structural characteristics influencing deformation capacity and plasticity in reinforced ductile cement-based composite structural components', *Composite Structures*. **224** (2019) 111013.

[6] Pokhrel, M., and Bandelt, M. J., 'Plastic hinge region and rotation capacity in reinforced HPFRCC flexural members at collapse level', in Proceedings of the Seventh International Colloquium on Performance, Protection & Strengthening of Structures under Extreme Loading & Events, Whistler, Canada, 2019. 1-15.

[7] Yoo, D. Y., and Yoon, Y. S., 'Structural performance of ultra-high-performance concrete beams with different steel fibers', *Engineering Structures*. **102** (2015) 409-423.

[8] Bandelt, M. J., and Billington, S. L., 'Impact of reinforcement ratio and loading type on the deformation capacity of high-performance fiber-reinforced cementitious composites reinforced with mild steel', *Journal of Structural Engineering*. **142** (10) (2016) 04016084.

[9] Bandelt, M. J., and Billington, S. L., 'Simulation of deformation capacity in reinforced high-performance fiber-reinforced cementitious composite flexural members', *Journal of Structural Engineering*. **144** (10) (2018) 04018188.
[10] Shao, Y., and Billington, S. L., 'Flexural performance of steel-reinforced engineered cementitious composites with different reinforcing ratios and steel types', *Construction and Building Materials.* **231** (2020) 117159.
[11] Bandelt, M. J., and Billington, S. L., 'Bond behavior of steel reinforcement in high-performance fiber-reinforced cementitious composite flexural members', *Materials and Structures*. **49** (1-2) (2016) 71-86.
[12] Lee, J., 'Bonding behavior of lap-spliced reinforcing bars embedded in ultra-high strength concrete with steel fibers', *KSCE Journal of Civil Engineering*, **20** (1) (2016) 273-281.
[13] Dagenais, M. A., and Massicotte, B., 'Cyclic behavior of lap splices strengthened with ultra high performance fiber-reinforced concrete', *Journal of Structural Engineering*. **143** (2) (2017) 04016163.
[14] Moreno, D. M., Trono, W., Jen, G., Ostertag, C., and Billington, S. L., 'Cement & Concrete Composites Tension stiffening in reinforced high performance fiber reinforced cement-based composites', *Cement and Concrete Composites*. **50** (2014) 36-46.
[15] Hung, C., Lee, H., and Nga, S., 'Tension-stiffening effect in steel-reinforced UHPC composites : Constitutive model and effects of steel fibers, loading patterns, and rebar sizes', *Composites Part B: Engineering*. **158** (2019) 269-278.
[16] Shao, Y., and Billington, S. L., 'Utilizing full UHPC compressive strength in steel reinforced UHPC beams', in Proceedings of Second International Interactive Symposium on Ultra-High Performance Concrete, Albany, New York, USA, 2019. 1-9.
[17] Shao, Y. and Billington, S. L., 'Predicting the two predominant flexural failure paths of longitudinally reinforced high-performance fiber-reinforced cementitious composite structural members', *Engineering Structures*. **199** (2019) 109581.
[18] ASTM, 'Standard practice for fabricating and testing specimens of ultra-high performance concrete', *ASTM C1856/C1586-17*. (2017) 1-4.
[19] Pokhrel, M., and Bandelt, M. J., 'Simulation of reinforced HPFRCC deformation capacity under flexure- and shear-dominated stress states', in Proceedings of Computational Modelling of Concrete and Concrete Structures, Bad Hofgastein, Austria, 2018. 633-640.
[20] Pokhrel, M. and Bandelt, M. J., 'Plastic hinge behavior and rotation capacity in reinforced ductile concrete flexural members', *Engineering Structures*. 200 (2019) 109699.